Inorg. Chem. **2007**, *46*, 10639–10646

Photoelectron Spectroscopy and Electronic Structure Calculations of d^1 Vanadocene Compounds with Chelated Dithiolate Ligands: Implications for Pyranopterin Mo/W Enzymes

Matthew A. Cranswick, Alice Dawson, J. Jon A. Cooney, Nadine E. Gruhn, Dennis L. Lichtenberger,* and John H. Enemark*

Department of Chemistry, The University of Arizona, Tucson, Arizona 85721

Received July 6, 2007

Gas-phase photoelectron spectroscopy and density functional theory have been used to investigate the electronic structures of open-shell bent vanadocene compounds with chelating dithiolate ligands, which are minimum molecular models of the active sites of pyranopterin Mo/W enzymes. The compounds Cp_2V(dithiolate) [where dithiolate is 1,2-ethenedithiolate ($S_2C_2H_2$) or 1,2-benzenedithiolate (bdt), and Cp is cyclopentadienyl] provide access to a 17-electron, d^1 electron configuration at the metal center. Comparison with previously studied Cp_2M(dithiolate) complexes, where M is Ti and Mo (respectively d^0 and d^2 electron configurations), allows evaluation of d^0, d^1, and d^2 electronic configurations of the metal center that are analogues for the metal oxidation states present throughout the catalytic cycle of these enzymes. A "dithiolate-folding effect" that involves an interaction between the vanadium d orbitals and sulfur p orbitals is shown to stabilize the d^1 metal center, allowing the d^1 electron configuration and geometry to act as a low-energy electron pathway intermediate between the d^0 and d^2 electron configurations of the enzyme.

Introduction

The bent metallocene class of molecules ($Cp_2M(L)_2$, Cp = η^5-cyclopentadienyl) provides access to many small molecules that contain metal-dithiolate ligation,[1] and are therefore useful as models of the pyranopterin-dithiolate system of the mononuclear molybdenum-containing enzymes that catalyze a wide range of oxidation/reduction reactions in carbon, sulfur, and nitrogen metabolism.[2−6] This class of molecules allows access to d^0 (M = Ti, Hf, Zr), d^1 (M = V, Nb), and d^2 (M = Mo, W) metal electron configurations, the same electron configurations as the metal center during the enzyme catalytic cycle. Bent metallocenes are known with a variety of different dithiolate ligands, many of which have been crystallographically characterized.[1] A common structural motif of metallocene dithiolates is a folding along the S···S vector, as illustrated in Figure 1.[7] Interestingly, the range of fold angles observed for metallocene dithiolates encompasses the range of fold angles that has also been observed in protein crystal structures of pyranopterin-dithiolate sites (7−30°).[8−12] The exact role of the pyranopterindithiolate coordination in the overall catalytic cycle of molybdenum enzymes is not yet established,[13] but the unusual ability of ene-1,2-dithiolate ligands to stabilize metals in multiple oxidation states has long been recognized.[14,15]

* To whom correspondence should be addressed. E-mail: dlichten@email.arizona.edu (D.L.L.); jenemark@email.arizona.edu (J.H.E.).

(1) Fourmigué, M. *Coord. Chem. Rev.* **1998**, *178*−*180*, 823−864.
(2) Rajagopalan, K. V.; Johnson, J. L. *J. Biol. Chem.* **1992**, *267*, 10199−10202.
(3) Hille, R. *Chem. Rev.* **1996**, *96*, 2757−2816.
(4) Sigel, A.; Sigel, H. In *Molybdenum and Tungsten: Their Roles in Biological Processes*; Metal Ions in Biological Systems; Dekker: New York, 2002; Vol. 39.
(5) Garner, D. C.; Banham, R.; Cooper, S. J.; Davies, E. S.; Stewart, L. J. *Handb. Metalloproteins* **2001**, 1023−1090.
(6) Burgmayer, S. J. N. *Prog. Inorg. Chem.* **2004**, *52*, 491−537.
(7) The fold angle is the acute angle between the vector from the metal to the centroid of the two sulfur atoms and the vector from this centroid to that of the two carbon atoms of the metallacycle.
(8) Kisker, C.; Schindelin, H.; Pacheco, A.; Wehbi, W.; Garrett, R. M.; Rajagopalan, K. V.; Enemark, J. H.; Rees, D. C. *Cell* **1997**, *91*, 973−983.
(9) Rebelo, J. M.; Dias, J. M.; Huber, R.; Moura, J. J. G.; Romão, M. J. *J. Biol. Inorg. Chem.* **2001**, *6*, 791−800.
(10) Enroth, C.; Eger, B. T.; Okamoto, K.; Nishino, T.; Nishino, T.; Pai, E. F. *Proc. Natl. Acad. Sci. U.S.A.* **2000**, *97*, 10723−10728.
(11) Li, H.; Temple, C.; Rajagopalan, K. V.; Schindelin, H. *J. Am. Chem. Soc.* **2000**, *122*, 7673−7680.
(12) Joshi, H. K.; Cooney, J. J. A.; Inscore, F. E.; Gruhn, N. E.; Lichtenberger, D. L.; Enemark, J. H. *Proc. Natl. Acad. Sci. U.S.A.* **2003**, *100*, 3719−3724.
(13) Schindelin, H.; Kisker, C.; Rees, D. C. *J. Biol. Inorg. Chem.* **1997**, *2*, 773−781.
(14) Eisenberg, R. *Prog. Inorg. Chem.* **1970**, *12*, 295−369.

10.1021/ic701338s CCC: $37.00
Published on Web 11/15/2007

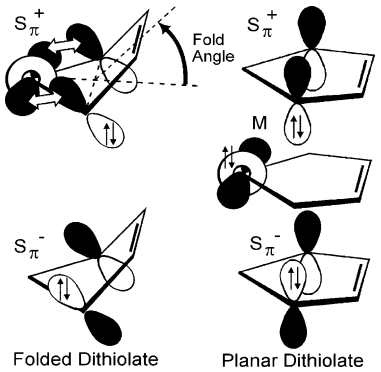

Figure 1. Representations of the valence orbitals of folded versus flat dithiolates. In the d^0 case, the metal orbital (M) is empty, and the S_π^+ orbital can interact upon folding. In the d^2 case the metal orbital (M) is filled, and a planar orientation minimizes a filled−filled interaction. The S_π^- orbital does not have the correct symmetry to interact with the metal orbital.

Proposed functions for the pyranopterin-dithiolate ligand include acting as an electron-transfer conduit from the metal to other prosthetic groups[16] and/or acting as a modulator of the oxidation/reduction potential of the metal site.[16,17] Modeling of the active site of the mononuclear molybdenum enzymes with small molecules has revealed useful information about the activity of these enzymes.[18]

A general bonding description of Cp_2MX_2 compounds is well understood,[19−21] and Lauher and Hoffmann first explained the variation in fold angle for Cp_2M(dithiolate) compounds as due to the occupancy of the metal d-orbital in the equatorial plane (or metal in-plane orbital, M_{ip}) with respect to the dithiolate ligand. This orbital is empty for the d^0 molecules, in which the metallocycle is folded along the S···S vector, and filled for the d^2 molecules, in which the metallocycle is nearly planar. The observed folding for the d^0 systems facilitates interaction of the filled S_π orbitals with the empty M_{ip} orbital, as shown in Figure 1. In the case of Cp_2Ti(bdt), which has a formally Ti(IV) d^0 metal center, the dithiolate ligand can be thought of as a six-electron donor. Each of the thiolate σ-orbitals provides two electrons, and two additional electrons come from the symmetric (S_π^+) orbital. Thus, folding the dithiolate ligand effectively stabilizes Cp_2Ti(bdt) as an 18-electron complex.[22,23] In contrast, for the d^2 metal system, folding of the ligand would bring a filled S_π orbital into close proximity with the filled M_{ip} orbital; the observed nearly planar metallocycle minimizes the filled−filled interaction between the ligand and metal-based orbitals.[12]

Previously, we have investigated the electronic structures of the d^0 and d^2 metal centers of the metallocene dithiolates as active site models for molybdopterin enzymes.[12,22] This study examines the d^1 metal electron configuration that is observed for molybdopterin enzymes, and its role as an intermediate in facilitating electron transfer between the d^0 and d^2 electron configurations of the enzyme active site. The electronic structures of the compounds Cp_2V(dithiolate) [where dithiolate is 1,2-ethenedithiolate ($S_2C_2H_2$), 1,2-benzenedithiolate (bdt), and Cp is cyclopentadienyl] are examined by gas-phase photoelectron spectroscopy (PES) and density functional theory (DFT). This study fills in the connection between our previous studies of Cp_2M(dithiolate) (M = Mo, Ti) that investigated the respective electronic structures of d^2 and d^0 metal centers. Investigation of Cp_2V-(dithiolate) as a model of the intermediate d^1 electron configuration of pyranopterin Mo/W enzymes leads to a basic understanding of how the electronic and geometric structures of the d^0, d^1, and d^2 electron configurations facilitate electron transfer to and from the enzyme active site.

Experimental Methods

General. Electronic absorption (dichloromethane solutions on a modified Cary 14 with OLIS interface, 280−1280 nm) and mass spectrometry (direct ionization on a JEOL HX110) were used to identify the compounds. The compound Cp_2V(bdt) was synthesized according to published procedures[24] and under anaerobic conditions using a glove box. Cp_2V (Strem), Cp_2VCl_2 (Aldrich), anhydrous THF (DriSolv), and anhydrous hexane (DriSolv) were used as supplied. The EPR spectrum of $Cp_2V(S_2C_2H_2)$ was obtained at X-band at 77 K on a Bruker 300E spectrometer in the Electron Paramagnetic Resonance Facility at The University of Arizona. The X-ray crystallographic structure of $Cp_2V(S_2C_2H_2)$ was determined by the Molecular Structure Laboratory at The University of Arizona.

Synthesis of $Cp_2V(S_2C_2H_2)$. To a suspension of freshly prepared $Na_2(S_2C_2H_2)$[25] (0.068 g, 0.5 mmol) in THF (5 mL) was added a suspension of Cp_2VCl_2 (0.126 g, 0.5 mmol) in THF (8 mL). The mixture was stirred for 2 h and allowed to stand overnight at room temperature. The red-purple mixture was then filtered, evaporated to dryness under vacuum, and washed with hexane (3 × 4 mL) to remove a blue impurity. The residue was dissolved in the minimum volume of THF (∼8 cm^3), layered with hexane (∼10 mL), and allowed to stand overnight at room temperature, then refrigerated at −20 C for 3 days to yield dark purple block crystals suitable for crystallography. Yield: 0.052 g, 40%. UV/vis/near-IR: 10800 (ϵ = 400), 12900 (140) sh, 18400 (520), 21700 (310) sh, 23700 (210), 24900 cm^{-1} (400 M^{-1} cm^{-1}) shoulder, and very intense UV transitions starting at 27500 cm^{-1}. EPR: $g_1 = 2.007$, $g_2 = 1.995$, $g_3 = 1.995$, $A_1 = 55.3$, $A_2 = 25.1$, $A_3 = 93.3$ (10^{-4} cm^{-1}). MS calculated *m*/*z* for $VS_2C_{12}H_{12}$: 270.9820 (100), obsd 270.9822 (100); calcd 271.9850 (15.12), obsd 271.9863 (16.35); calcd 272.9789 (9.92), obsd 272.9784 (10.64% normalized intensity).

X-ray Crystallographic Analysis. Data were collected for Cp_2V-$(S_2C_2H_2)$ on a Bruker SMART 1000 CCD detector X-ray diffractometer. The structure was solved using SIR92.[26] Refinements were

(15) In *Dithiolene Chemistry: Synthesis, Properties, and Applications*; Karlin, K. D., Stiefel, E. I., Eds.; *Progress in Inorganic Chemistry*; John Wiley and Sons, Inc.: Hoboken, NJ, 2004; Vol. 52, pp 738.
(16) Inscore, F. E.; McNaughton, R.; Westcott, B.; Helton, M. E.; Jones, R.; Dhawan, I. K.; Enemark, J. H.; Kirk, M. L. *Inorg. Chem.* **1999**, *38*, 1401−1410.
(17) Westcott, B. L.; Gruhn, N. E.; Enemark, J. H. *J. Am. Chem. Soc.* **1998**, *120*, 3382−3386.
(18) Enemark, J. H.; Cooney, J. J. A.; Wang, J. J.; Holm, R. H. *Chem. Rev.* **2004**, *104*, 1175−1200.
(19) Lauher, J. W.; Hoffmann, R. *J. Am. Chem. Soc.* **1976**, *98*, 1729−1742.
(20) Green, J. C. *Chem. Soc. Rev.* **1998**, *27*, 263−272.
(21) Green, J. C. *Struct. Bonding* **1981**, *43*, 37−112.
(22) Cooney, J. J. A.; Cranswick, M. A.; Gruhn, N. E.; Joshi, H. K.; Enemark, J. H. *Inorg. Chem.* **2004**, *43*, 8110−8118.
(23) Pyykko, P. *J. Organomet. Chem.* **2006**, *691*, 4336−4340.
(24) Stephan, D. W. *Inorg. Chem.* **1992**, *31*, 4218−4223.
(25) King, R. B.; Eggers, C. A. *Inorg. Chem.* **1968**, *7*, 340−345.
(26) Altomare, A.; Cascarano, G.; Giacovazzo, C.; Guagliardi, A. *J. Appl. Crystallogr.* **1993**, *26*, 343−350.

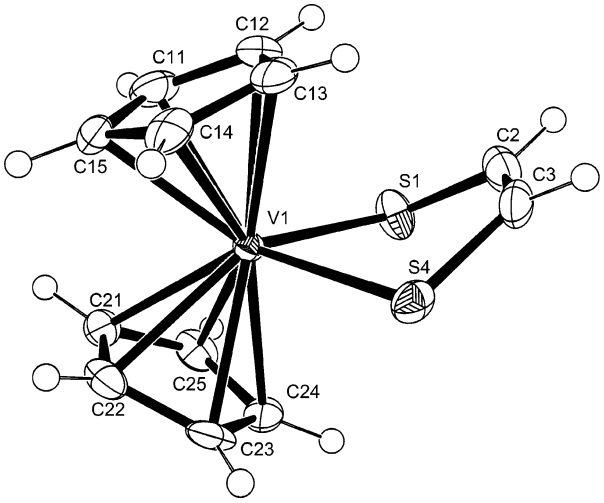

Figure 2. ORTEP representation of $Cp_2V(S_2C_2H_2)$ with 50% thermal ellipsoids.

performed using SHELXL,[27] and illustrations were made using XP. Solution was achieved utilizing direct methods followed by Fourier synthesis. Hydrogen atoms were added at idealized positions, constrained to ride on the atom to which they are bonded, and given thermal parameters equal to $1.2U_{iso}$ of that bonded atom. A parameter describing extinction was included, but refined to zero and was removed prior to final refinement cycles. The final anisotropic full-matrix least-squares refinement based on F^2 of all reflections converged (maximum shift/esd = 0.000) at R1 = 0.0644, wR2 = 0.0986, and goodness-of-fit = 1.040. "Conventional" refinement indices using the 1972 reflections with $F > 4\sigma(F)$ are R1 = 0.0389, wR2 = 0.0855. The model consisted of 136 variable parameters; no restraints were used. There were no correlation coefficients greater than 0.50. The highest peak on the final difference map was 0.495 e Å^{-3} located 0.82 Å from S1. The lowest peak on the final difference map was −0.343 e Å^{-3} located 0.72 Å from C2. Scattering factors and anomalous dispersion were taken from International Tables Vol. C, Tables 4.2.6.8 and 6.1.1.4.

Photoelectron Spectroscopy. Photoelectron spectra were recorded using an instrument, procedures, and calibration that have been described in detail previously.[28] The electron detection and instrument operation are interfaced to a National Instruments PCIe-6259 multifunction data acquisition card and custom software. During data collection, the instrument resolution (measured using fwhm of the argon $^2P_{3/2}$ peak) was 0.020−0.030 eV. The sublimation temperatures (at 10^{-5} Torr, monitored using a "K" type thermocouple passed through a vacuum feed-through and attached directly to the sample cell) were 190−200 °C for $Cp_2V(S_2C_2H_2)$ and 195−210 °C for Cp_2V(bdt). The samples sublimed cleanly without evidence of decomposition. In Figure 3, the vertical length of each data mark represents the experimental variance of that point. The valence ionization bands in the He I spectra are represented analytically with the best fit of asymmetric Gaussian peaks as described previously.[29] The peak positions are reproducible to about ±0.02 eV (≈3σ). The analytical ionization bands that model the He I spectra are also used to model the ionizations in the He II spectra, with only the intensities of the analytical bands allowed to vary to account for the changes in photoelectron cross-sections with the change in excitation source energy from He I to He II.

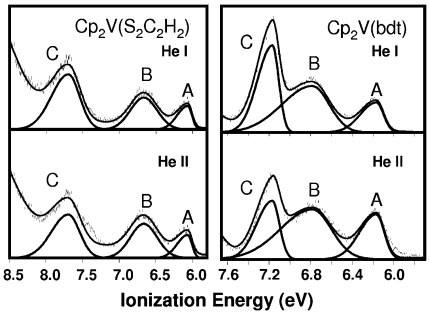

Figure 3. Low-energy valence region of the gas-phase photoelectron spectra of $Cp_2V(S_2C_2H_2)$ and Cp_2V(bdt) with He I and He II excitation. Band C is due to the S_π^- orbital, B is the S_π^+/V bonding orbital, and A is the singly occupied S_π^+/V antibonding orbital.

Computational Methods. The Amsterdam Density Functional theory suite (ADF 2006.01b, using default parameters except for the options given in parentheses) was used to study the electronic structures of $Cp_2M(S_2C_2H_2)$ and Cp_2M(bdt), where M is V and Mo.[30−34] The optimized geometries of $Cp_2V(S_2C_2H_2)$, Cp_2V(bdt), and Cp_2Mo(bdt) (Tables S1−S3, respectively, in Supporting Information) were obtained in C_s symmetry. $Cp_2V(S_2C_2H_2)$, Cp_2V(bdt), and Cp_2Mo(bdt) were constructed such that the Cp rings were staggered with respect to each other, as similarly found in the crystal structure, and such that the C_s plane was coincident with the *xy*-plane. In $Cp_2V(S_2C_2H_2)$, Cp_2V(bdt), and Cp_2Mo(bdt), the C_s plane bisects the metal atom and all three ligands. A generalized gradient approximation, with the correlation of Perdew et al.[35] and exchange correction of Handy and Cohen[36] (GGA OPBE), was used for calculations of the optimized geometries. The calculations employed double- or triple-ζ basis sets with Slater type orbitals and polarization functions for all elements (DZP for C, H, and S and TZP for V and Mo). Higher level basis sets did not give significantly different results for comparison of ionization energies. Calculations on the ground-state molecules were performed in the spin-unrestricted mode since each molecule contains one unpaired electron. Relativisitic effects were considered for all atoms by using the zero-order regular approximation (relativistic scalar ZORA).[37,38] The numerical integrals in ADF were evaluated to six significant figures (integration = 6.0), and the convergence criteria of the energy, gradients, and estimated coordinate uncertainty were tightened (converge E = 0.001, grad = 0.001, rad = 0.001). The self-consistent field (SCF) convergence limits were also tightened (convergence 1e-6 1e-6). Analytical frequency calculations (AnalyticalFreq) were also carried out on the optimized geometry of Cp_2Mo(bdt), and there were no imaginary frequencies.

ΔSCF calculations of the ionized states were performed at the fixed geometry of the neutral molecule, with one electron removed

(27) Sheldrick, G. M. In *SHELXL97*; University of Göttingen: Göttingen, Germany, 1997.
(28) Lichtenberger, D. L.; Kellogg, G. E.; Kristofzski, J. G.; Page, D.; Turner, S.; Klinger, G.; Lorenzen, J. *Rev. Sci. Instrum.* **1986**, *57*, 2366.
(29) Lichtenberger, D. L.; Copenhaver, A. S. *J. Electron. Spectrosc. Relat. Phenom.* **1990**, *50*, 335−352.
(30) Baerends, E. J.; Ellis, D. E.; Ros, P. *Chem. Phys.* **1973**, *2*, 41−51.
(31) Fonseca Guerra, C.; Snijders, J. G.; te Velde, G.; Baerends, E. J. *Theor. Chem. Acc.* **1998**, *99*, 391−399.
(32) te Velde, G.; Bickelhaupt, F. M.; Baerends, E. J.; Fonseca Guerra, C.; Van Gisbergen, S. J. A.; Snijders, J. G.; Ziegler, T. *J. Comput. Chem.* **2001**, *22*, 931−967.
(33) te Velde, G.; Baerends, E. J. *J. Comput. Phys.* **1992**, *99*, 84−98.
(34) Versluis, L.; Ziegler, T. *J. Chem. Phys.* **1988**, *88*, 322−329.
(35) Perdew, J. P.; Burke, K.; Wang, Y. *Phys. Rev. B* **1996**, *54*, 16533−16539.
(36) Handy, N. C.; Cohen, A. J. *Mol. Phys.* **2001**, *99*, 403−412.
(37) Vanlenthe, E.; Baerends, E. J.; Snijders, J. G. *J. Chem. Phys.* **1993**, *99*, 4597−4610.
(38) Vanlenthe, E.; Baerends, E. J.; Snijders, J. G. *J. Chem. Phys.* **1994**, *101*, 9783−9792.

Table 1. X-ray Crystallographic Parameters of $Cp_2V(S_2C_2H_2)$

empirical formula	$C_{12}H_{12}S_2V$
fw	271.28
T	170(2) K
wavelength	0.71073 Å
cryst syst	monoclinic
space group	$P2_1/c$
unit cell dimensions	$a = 11.3051(10)$ Å
	$b = 7.5236(7)$ Å
	$c = 13.3767(12)$ Å
	$\beta = 104.849(2)°$
V	1099.76(17) Å^3
Z	4
density (calcd)	1.638 Mg/m^3
abs coeff	1.240 mm^{-1}
reflns utilized	12814
indep reflns	2675 [R(int) = 0.0497][a]
final R indices [$I > 2\sigma(I)$]	R1 = 0.0389, wR2 = 0.0855[a]
R indices (all data)	R1 = 0.0644, wR2 = 0.0986[a]

[a] $R(\text{int}) = \sum|F_o^2 - \langle F_o^2\rangle|/\sum[F_o^2]$, $R1 = \sum||F_o| - |F_c||/\sum|F_o|$, $wR2 = \{\sum[w(F_o^2 - F_c^2)^2]/\sum[w(F_o^2)^2]\}^{1/2}$, $w = 1/[\sigma^2(F_o^2) + (0.0466P)^2]$ where $P = (F_o^2 + 2F_c^2)/3$.

from the relevant orbital. The first positive ion of each molecule is a closed-shell singlet, but the higher positive ion states (corresponding to ionization of electrons from orbitals below the HOMO) contain two unpaired electrons and were calculated as both spin-unrestricted singlets and triplets. The ΔSCF estimate of the ionization energy is the difference between the calculated total energy of the ionized state and that of neutral ground state molecule.

Fold angle potential curves were created by utilizing the Linear Transit option in the Geometry block along with the Geovar keyword. Linear Transit calculations were run such that the fold angle was fixed every 5° or 10° through some range (e.g., 60° to −60°), and all geometric parameters, other than the fold angle, were allowed to fully optimize at each step.

Results and Discussion

Crystallography. There is one crystallographically independent molecule in the structure of $Cp_2V(S_2C_2H_2)$. The structure (Figure 2, Tables 1 and S4) is similar to that of $Cp_2V(bdt)$, as published by Stephan.[24] Two cyclopentadienyl rings and two sulfur atoms complete a pseudotetrahedral coordination sphere of vanadium. The ene-dithiolate chelates to the V center through the two S atoms and shows folding along the S···S vector as illustrated in Figure 1, with a fold angle of 38.5°. The V−C and V−S distances average 2.302 and 2.425 Å, respectively. These compare with the V−C and V−S distances published for $Cp_2V(bdt)$ (2.30 and 2.431 Å).[24] The S1−V−S2 angle of 81.14 (3)° is similar to that of 79.8° in $Cp_2V(bdt)$.[24] It is interesting to note that the bond lengths for the analogous titanium compounds are longer for M−C(Cp) (2.387 Å for $Cp_2Ti(S_2C_2H_2)$ and 2.37 Å for $Cp_2Ti(bdt)$) whereas the M−S bond lengths and S−M−S angles are very similar (2.417 Å and 83.23° for $Cp_2Ti(S_2C_2H_2)$ and 2.416 Å and 82.2° for $Cp_2Ti(bdt)$). The trend of Cl−M−Cl angles for Cp_2MCl_2 compounds is Ti/Zr > V/Nb > Mo.[39,40] This trend is not echoed for $Cp_2M(bdt)$ (M = Ti, V, and Mo) with the S−M−S angles of: 82.0°, 79.8°, and 82.1°, respectively. The effect of the electron density along the z-axis is overpowered, presumably, by the formation of the chelate ring.

EPR. Previous studies of Cp_2VX_2 (where X is a monoanionic ligand, such as an alkyl or halide) have utilized electron paramagnetic resonance (EPR) to determine the molecular orbital character of the vanadium d^1 electron. The EPR spectrum of $Cp_2V(S_2C_2H_2)$ (Figure S2) is similar to that of Cp_2VCl_2 reported previously.[39−42] The trend of the Cl−M−Cl angle to decrease with M, changing from Ti to V to Mo, and single-crystal EPR studies led to the conclusion that the HOMO of the V and Mo compounds is primarily along an axis normal to the plane bisecting the Cl−M−Cl angle. Lowering the symmetry from C_{2v} to C_s allows this axis to be labeled z, and the orbital was calculated as $|\Psi_0> = a|d_{z^2}> + b|d_{x^2-y^2}>$, where $a = -0.963$ and $b = 0.270$ (Mulliken charges, $a^2{:}b^2 = 20.5{:}1$) for Cp_2VCl_2.[40] This is close to the observed $a = -0.976$ and $b = 0.218$ ($a^2{:}b^2$ 20.0:1) for $(C_5H_4Me)_2VCl_2$. These EPR parameters have been compared with those of Cp_2VCl_2, calculated as Mulliken charges.[40] Using more current methods, a similar comparison can be made between the observed EPR and orbital percent characters calculated by DFT. For Cp_2VCl_2, the singly occupied, spin α orbital percent character is calculated to be 60.8% d_{z^2} and 3.44% $d_{x^2-y^2}$ giving a ratio of 17.7:1.[43] This is in agreement with previous experiments (see above) concluding that the singly occupied orbital is of primarily d_{z^2} character.

The higher g values and lower $A(^{51}V)$ values of $Cp_2V(S_2C_2H_2)$ reflect the softer coordination environment and covalent nature of the dithiolate ligand compared to the two chloride ligands in Cp_2VCl_2. Previous studies of Tp*MoOXY (where Tp* = hydrotris(3,5-dimethyl-1-pyrazolyl)borate; (X,Y) = Cl, or toluenedithiol (tdt)) exhibit a similar trend in the g and $A(^{95,97}Mo)$ values with a change in the coordination sphere.[44] The higher g values and lower $A(^{95,97}Mo)$ values of Tp*MoO(tdt) compared to Tp^*MoOCl_2 are attributed to a low-energy charge-transfer transition in Tp*MoO(tdt) (9010 cm^{-1}, $\epsilon = 520$) that can mix sulfur character into the ground state.[44] Tp^*MoOCl_2 does not exhibit a similar charge-transfer transition, but has a d → d transition as the lowest energy band. In a comparison of the electronic spectra of Cp_2VCl_2 and $Cp_2V(S_2C_2H_2)$ (Figure S3), there is a low-energy ligand-to-metal charge-transfer transition[15] for $Cp_2V(S_2C_2H_2)$ (10800 cm^{-1}, $\epsilon = 400$), but Cp_2VCl_2 lacks a similar low-energy transition. The difference in the low-energy charge-transfer transitions between Cp_2VCl_2 and $Cp_2V(S_2C_2H_2)$ would account for the greater g and lower $A(^{51}V)$ values exhibited by $Cp_2V(S_2C_2H_2)$ compared to Cp_2VCl_2.[45,46]

(39) Petersen, J. L.; Dahl, L. F. *J. Am. Chem. Soc.* **1974**, *96*, 2248−2250.
(40) Petersen, J. L.; Lichtenberger, D. L.; Fenske, R. F.; Dahl, L. F. *J. Am. Chem. Soc.* **1975**, *97*, 6433−6441.
(41) Petersen, J. L.; Dahl, L. F. *J. Am. Chem. Soc.* **1975**, *97*, 6416−6422.
(42) Petersen, J. L.; Dahl, L. F. *J. Am. Chem. Soc.* **1975**, *97*, 6422−6433.
(43) Cranswick, M. A.; Gruhn, N. E.; Enemark, J. H.; Lichtenberger, D. L. Submitted to *Journal of Organometallic Chemistry*.
(44) Cleland, W. E., Jr.; Barnhart, K. M.; Yamanouchi, K.; Collison, D.; Mabbs, F. E.; Ortega, R. B.; Enemark, J. H. *Inorg. Chem.* **1987**, *26*, 1017−1025.
(45) Stewart, C. P.; Porte, A. L. *Dalton Trans.* **1973**, *7*, 722−729.
(46) Bakalik, D. P.; Hayes, R. G. *Inorg. Chem.* **1972**, *11*, 1734−1738.

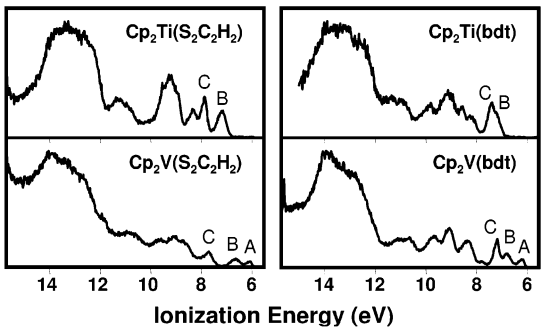

Figure 4. The spectra of $Cp_2V(S_2C_2H_2)$ and $Cp_2V(bdt)$ have one more band (band A) than their respective titanocene analogues.

Photoelectron Spectroscopy. Spectroscopic evidence supporting the Lauher and Hoffmann[19] description of the electronic structure includes our recent PES study of the nearly planar metallocycle, $Cp_2Mo(bdt)$,[12] and the folded metallocycle, $Cp_2Ti(bdt)$, for which ionizations from primarily metal-based orbitals and primarily S p_π-based orbitals can be experimentally distinguished from one another.[12,22,47] The S p_π-based orbitals of the two sulfur atoms form a symmetric and antisymmetric pair. The symmetric (S_π^+) orbital combination has the right symmetry and energy to match the M_{ip} orbital upon folding of the dithiolate unit, whereas the antisymmetric sulfur (S_π^-) orbital combination does not (Figure 1). The substantial mixing of the out-of-plane S_π^+ orbital and the M_{ip} orbital upon folding is shown experimentally in the PE spectra of $Cp_2Ti(bdt)$ by the increase in intensity of the S_π^+ ionization band relative to the S_π^- ionization band with change in ionization source energy from He I to He II. In order for this "dithiolate-folding effect" to be present, there must be effective coupling between the S p_π orbitals and the C p_π orbitals derived from the ene-dithiolate ligand backbone.[22] Such coupling raises the energy of the S_π^+ orbital above that of the S_π^- orbital, and poises the energy of the S_π^+ orbital for interaction with the metal-based in-plane orbital (M_{ip}). This electronic structure facilitates the "dithiolate-folding effect" as only the S_π^+ orbital has the correct symmetry to overlap with the metal-based in-plane orbital. For example, we have previously shown that $Cp_2Ti(bdt)$ and $Cp_2Ti(S_2C_2H_2)$, which both have an unsaturated carbon−carbon bond linking the two S atoms, show a dithiolate-folding effect. However, if a saturated dithiolate ligand is present, such as in $Cp_2Ti(S_2C_3H_6)$,[22] the coupling between the pπ orbitals on the two S atoms is greatly reduced and the ordering of the S_π orbitals is reversed in comparison to the unsaturated dithiolate.

The low-energy valence regions of the gas-phase photoelectron spectra of $Cp_2V(S_2C_2H_2)$ and $Cp_2V(bdt)$, collected with both He I and He II photon sources, are presented in Figure 3. Comparison of the He I spectra with their titanocene analogues[22] in Figure 4 reveals a similar overall ionization profile in each case, except for the presence of the weak band A at low energy (6.06 and 6.17 eV for $Cp_2V(S_2C_2H_2)$ and $Cp_2V(bdt)$, respectively), as expected for the additional electron in the vanadium complexes.

(47) Joshi, H. K. Ph.D. Dissertation, The University of Arizona, Tucson, AZ, 2003.

Table 2. Ionization Energies, Band Shapes, and He I and He II Band Areas for $Cp_2V(S_2C_2H_2)$ and $Cp_2V(bdt)$

				relative area[a]	
band	I.E.[b] (eV)	bandwidth high (eV)	bandwidth low (eV)	He I	He II
		$Cp_2V(S_2C_2H_2)$			
A	6.06	0.34	0.14	1	1
B	6.67	0.43	0.43	2.46	2.69
C	7.70	0.54	0.36	4.41	3.58
		$Cp_2V(bdt)$			
A	6.17	0.36	0.16	1	1
B	6.78	0.69	0.38	3.15	2.28
C	7.17	0.34	0.14	2.65	1.20

[a] Areas are relative to band A. [b] Vertical ionization energy.

Table 2 lists the changes in areas of ionization bands B and C relative to the first ionization band A with change in ionization source from He I to He II for $Cp_2V(S_2C_2H_2)$ and $Cp_2V(bdt)$. From previous experimental studies[48−50] and calculations of atomic photoionization cross-sections,[51] it is expected that ionizations from molecular orbitals with significant Ti 3d contributions will increase in intensity compared to ionizations of primarily S 3p character when data collected with a He II photon source are compared to data collected with a He I photon source (Table 2). The changes in relative areas of the bands in $Cp_2V(S_2C_2H_2)$ and $Cp_2V(bdt)$ are similar, indicating that the atomic character of the molecular orbitals for the two molecules is similar. Band C in the titanocene dithiolate spectra is assigned to an S_π^- ionization, which does not mix significantly with the empty metal d acceptor orbital, and hence decreases in intensity significantly relative to the S_π^+ band (band B).[22] The destabilization of band B in the vanadocene dithiolate spectra compared to the related ionization in the titanocene spectra can be attributed to the interaction of the additional vanadium d^1 electron with the S_π^+ orbital, which decreases the fold angle and lowers the bonding interaction of S_π^+ with M_{ip}. Band C in the spectra of $Cp_2V(S_2C_2H_2)$ and $Cp_2V(bdt)$ decreases in intensity relative to both the first and second bands, and can therefore also be assigned to S_π^- (Table 2). Band C shows little change in ionization potential between the vanadocene and titanocene dithiolate spectra consistent with its nonbonding interaction with M_{ip}. Band A increases slightly with respect to band B in $Cp_2V(bdt)$ and decreases slightly in $Cp_2V(S_2C_2H_2)$, indicating mixing of metal and sulfur character and making absolute assignment difficult at this point. Comparison with the titanium analogues indicates that bands A and B both have mixed vanadium and S_π^+ character.

Computations. DFT calculations provide additional insight into the metal−ligand interactions for $Cp_2V(S_2C_2H_2)$ and $Cp_2V(bdt)$ indicating that upon dithiolate folding the mixing of metal d and sulfur p_π orbitals can be favored by their energy and symmetry match. The calculated molecular structures of $Cp_2V(S_2C_2H_2)$ and $Cp_2V(bdt)$ in general agree

(48) Glass, R. S.; Gruhn, N. E.; Lichtenberger, D. L.; Lorance, E.; Pollard, J. R.; Birringer, M.; Block, E.; DeOrazio, R.; He, C.; Shan, Z.; Zhang, X. *J. Am. Chem. Soc.* **2000**, *122*, 5065−5074.
(49) Green, J. C. *Acc. Chem. Res.* **1994**, *27*, 131−137.
(50) Gelius, U. *J. Electron. Spectrosc. Relat. Phenom.* **1974**, *5*, 985−1057.
(51) Yeh, J. J.; Lindau, I. *At. Data Nucl. Data Tables* **1985**, *32*, 1−155.

Table 3. Experimental and Calculated Orbital Ionization Energies (eV) for Bands A, B, and C of $Cp_2V(S_2C_2H_2)$ and Cp_2V(bdt)

			Kohn−Sham orbital energy[a]		ΔSCF[b]	
band	I.E.[c]	Label[d]	α-spin	β-spin	singlet	triplet
			$Cp_2V(S_2C_2H_2)$			
A	6.06	V d^1/S_π^+	−3.87		6.12	
B	6.67	V d^1/S_π^+	−4.91	−4.40	7.10	6.57
C	7.70	S_π^-	−5.68	−5.50	7.91	7.77
			Cp_2V(bdt)			
A	6.17	V d^1/S_π^+	−4.21		6.22	
B	6.78	V d^1/S_π^+	−5.21	−4.83	7.18	6.77
C	7.17	S_π^-	−5.36	−5.11	7.27	7.10

[a] The calculated orbital energy for the ground state. [b] The difference in total energy between molecular ground state, and the molecule with an electron removed from the specified orbital. [c] Experimental vertical ionization energy. [d] Primary character.

with the reported structures determined from X-ray crystallography (Table S4).[24,52] The Cp rings were staggered with respect to each other in the initial input guess geometries similar to the crystal structure of the ene-dithiolate complex and as determined to be a true minimum from the frequency analysis of the related Mo molecule. Rotation of the two Cp ligand rings has been shown to be a low-energy process,[53] and therefore, additional Cp orientations were not explored. The calculated fold angles for the coordinated dithiolates are smaller than those determined crystallographically. For $Cp_2V(S_2C_2H_2)$, the calculated angle is 29.9° and the experimental angle is 38.5°, and for Cp_2V(bdt) the calculated angle is 36.6° and the experimental angle is 41.0° and 40.1°.[24] Solid-state effects likely contribute to the differences between the calculated and crystallographic fold angles.[54]

The energies of the ionizations observed for $Cp_2V(S_2C_2H_2)$ and Cp_2V(bdt) by photoelectron spectroscopy are compared with those calculated by the ΔSCF method in Table 3. The ground states of the neutral molecules have $s = {}^1/_2$ (V^{4+}, d^1, $^2A'$); ionization from the SOMO will lead to a singlet state, but ionization from the doubly occupied orbitals leads to either singlet or triplet state configurations with singlet:triplet band relative intensities approximately 1:3. Table 3 shows the calculated values for the singlet and triplet states of $Cp_2V(S_2C_2H_2)$ and Cp_2V(bdt) using the ΔSCF method. For $Cp_2V(S_2C_2H_2)$, the calculated singlet/triplet state separation for band B is 0.53 eV and should be discernible in the experiment, although the band maximum will be dominated by the triplet state. The calculated energy for the formation of a triplet state (6.57 eV) agrees well with the observed ionization energy maximum for band B (6.67 eV), and no distinct ionization is observed for the singlet state. For band C, the calculated singlet/triplet state separation is 0.14 eV, which is less than the width of the vibrational manifolds associated with these ionizations, and a singlet state shoulder on the triplet state ionization is not observable. Again, the calculated vertical ionization for the triplet state (7.77 eV) agrees well with the observed band maximum for band C (7.70 eV).

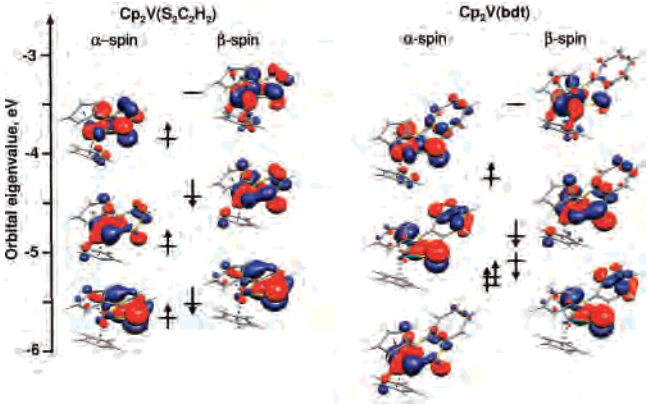

Figure 5. Spin correlation diagrams for $Cp_2V(S_2C_2H_2)$ and Cp_2V(bdt) showing α- and β-spin eigenvalues, molecular orbital character, and electron occupations based on ground state configuration.

A similar assignment is given for Cp_2V(bdt) based on the ΔSCF calculations. The increase in ionization energies for bands A and B and the decrease in ionization energy for band C from $Cp_2V(S_2C_2H_2)$ to Cp_2V(bdt) observed in the photoelectron spectra also is obtained from the calculations. The observed separation in energy between bands B and C is different for $Cp_2V(S_2C_2H_2)$ and Cp_2V(bdt) (1.03 and 0.39 eV, respectively) correlating with the separation in energy between the S_π^+ and S_π^- for their titanocene analogues (0.70 and 0.22 eV, for $Cp_2Ti(S_2C_2H_2)$ and Cp_2Ti(bdt), respectively). This trend, which is reproduced computationally, is presumably due to different inductive effects of the ligands and the greater involvement of the benzene ring in the π-system of the ligand for Cp_2V(bdt) and Cp_2Ti(bdt). In general, the calculated singlet/triplet separations for $Cp_2V(S_2C_2H_2)$ and Cp_2V(bdt) are small and within the experimental band widths for the ionizations, which is in agreement with previous studies of vanadium(IV) systems.[55,56]

Also included for comparison in Table 3 are the Kohn−Sham orbital energies for the α and β spin electrons. Early calculations of metal complexes with a partially filled metal d orbital bury the partially filled orbital below the filled ligand orbitals,[57−61] but in the present calculations the orbital ordering agrees with the calculated and observed sequence of ionizations. Contour plots of the spin α and β orbitals for $Cp_2V(S_2C_2H_2)$ and Cp_2V(bdt) that correspond to the ionizations evaluated by photoelectron spectroscopy are shown in Figure 5. The contour plots show that for $Cp_2V(S_2C_2H_2)$ and Cp_2V(bdt) the SOMOs are substantially delocalized with greater sulfur 3p character than vanadium d_{z^2} character, in agreement with the greater *g* and lower *A* values observed

(52) Tzavellas, N.; Klouras, N.; Raptopoulou, C. P. *Z. Anorg. Allg. Chem.* **1996**, *622*, 898−902.
(53) Cacelli, I.; Keogh, D. W.; Poli, R.; Rizzo, A. *J. Phys. Chem. A* **1997**, *101*, 9801−9812.
(54) Fourmigue, M. *Acc. Chem. Res.* **2004**, *37*, 179−186.
(55) Wescott, B. L.; Gruhn, N. E.; Michelsen, L. J.; Lichtenberger, D. L. *J. Am. Chem. Soc.* **2000**, *122*, 8083−8084.
(56) Gruhn, N. E.; Michelsen, L. J.; Westcott, B. L. *Inorg. Chem.* **2002**, *41*, 5907−5911.
(57) Doran, M.; Hillier, I. H.; Seddon, E. A.; Seddon, K. R.; Thomas, V. H.; Guest, M. F. *Chem. Phys. Lett.* **1979**, *63*, 612−614.
(58) Berry, M.; Garner, C. D.; Hillier, I. H.; Macdowell, A. A. *Inorg. Chem.* **1981**, *20*, 1962−1965.
(59) Dibella, S.; Gulino, A.; Lanza, G.; Fragala, I. L.; Marks, T. J. *J. Phys. Chem.* **1993**, *97*, 11673−11676.
(60) Di Bella, S.; Lanza, G.; Gulino, A.; Fragala, I. *Inorg. Chem.* **1996**, *35*, 3885−3890.
(61) DiBella, S.; Lanza, G.; Fragala, I. L.; Marks, T. J. *Organometallics* **1996**, *15*, 205−208.

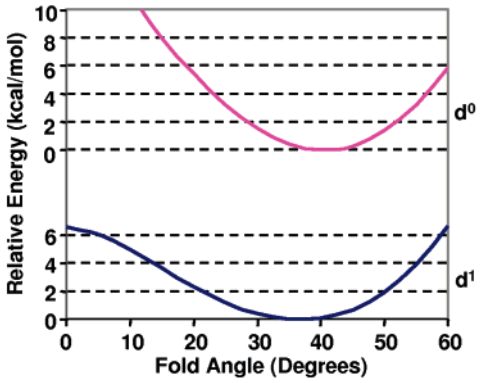

Figure 6. Potential energy diagrams showing the calculated total energy with change in fold angle for the neutral (d^1) and cation (d^0) of $Cp_2V(bdt)$.

in the EPR experiment. The contour plots for $Cp_2V(bdt)$ also show that the orbital character is extended onto the benzene π-system (the orbital percent contributions shown in Figure 5 are given in Table S5).

The description of these orbitals is consistent with the S_{π}^{+} and V d_{z^2} orbitals forming a bonding and antibonding pair of orbitals, as shown in Figure 5, where the SOMO is the antibonding combination and the next orbital is the doubly occupied bonding combination. This bonding/antibonding combination explains the strong vanadium and sulfur character mixing observed for bands A and B in the photoelectron spectra. Overall, the orbital picture corresponds to the bonding interaction proposed by Lauher and Hoffman.[19]

DFT calculations also offer insight into how the dithiolate-folding effect and the fold angle influence the oxidation/reduction and electron-transfer properties of the active site metal center. Using the linear transit option in the ADF package, potential energy curves for $Cp_2V(bdt)$ as neutral and cation molecules can be constructed to show how the fold angle changes with oxidation of the d^1 M_{ip} orbital. Figure 6 shows a fold angle potential energy curve plot for $Cp_2V(bdt)$ and $[Cp_2V(bdt)]^+$, where the change in relative energy with fold angle is compared. The potential energy curve of the neutral $Cp_2V(bdt)$ molecule shows that the energy minimum lies at approximately 37°. Oxidation of the M_{ip} orbital leads to an increase in the fold angle from 37° to 40°, resulting in a deeper potential well for the cation. The potential energy curve for the d^1 and d^0 electronic configurations of $Cp_2V(S_2C_2H_2)$ is similar (Figure S1).

Figure 7 presents the potential energy curves of the neutral (d^2), cation (d^1), and dication (d^0) of $Cp_2Mo(bdt)$ obtained from the gas-phase linear transit calculations with varying fold angle. The figure shows the calculated relative total energies between the optimized geometries of each electron configuration, along with the relative energy perturbation caused by dithiolate-folding for each electronic configuration (d^2, d^1, and d^0).[62] For $Cp_2Mo(bdt)$ the calculated fold angle

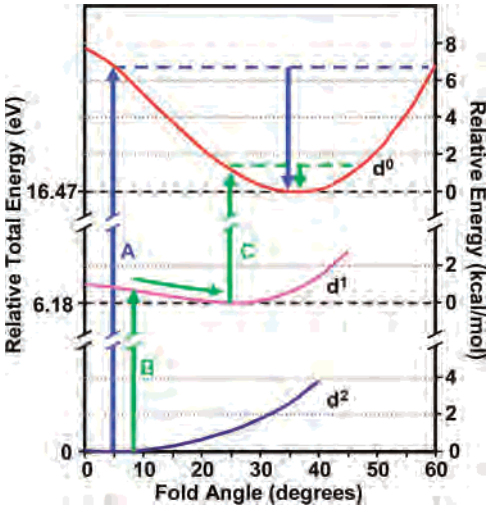

Figure 7. The gas-phase potential energy curve plots of the neutral (d^0), cation (d^1), and dication (d^2) of $Cp_2Mo(bdt)$ are shown with relative total energies (eV, left-hand side) and relative potential energies with change in fold angle (kcal/mol, right-hand side). The oxidation along path A (blue arrows and line) from the d^2 to d^0 electron configurations involves a large energy barrier to oxidation and larger reorganization energies with change in fold angle. Paths B and C (green arrows and lines) show the two-step two-electron oxidation of the d^2 to d^1 to d^0 electron configurations. Utilization of the shallow d^1 potential curve poises oxidation to occur with minimal reorganization energies with change in fold angle.

for the neutral (d^2) molecule exhibits a potential minimum at 0°. Upon oxidation from M_{ip} the fold angle increases to 25° for the cation (d^1), and to 35° for the dication (d^0). This range of fold angles is consistent with the DFT analysis by Domercq et al.[63] The analytical frequency calculations for $Cp_2Mo(bdt)$ show that the folding vibration is the lowest energy vibration in the molecule at 28 cm^{-1}; a nearly classical description of the vibronic states is appropriate for these curves, and thermal populations will be significant during electron transfer. This trend in the calculated fold angles for the $Cp_2Mo(bdt)$ series in Figure 7 follows that of the neutral d^2, d^1, and d^0 metallocene dithiolate crystal structures (vida supra).

Figure 7 not only shows the increase in fold angle with oxidation, but also gives insight into the role of the d^1 electron configuration in molybdopterin enzymes during substrate turnover. The relative energies between the d^2, d^1, and d^0 configurations will be reduced from the gas-phase values in Figure 7 by stabilization of the cations in the molybdopterin enzyme environment. Oxidation starting from the d^2 configuration and proceeding to the d^0 electron configuration without geometry reorganization along path A, followed by reorganization of the d^0 configuration to the minimum of the potential well (blue arrows and line in Figure 7), is a high-energy process with a large reorganization energy. The reorganization energy is approximately 0.26 eV (7 kcal mol^{-1}). Alternatively, oxidation from the d^2 to d^1 electron configurations allows access to the shallow d^1 potential with little reorganization energy investment upon changing the fold angle from 5° to 25° (arrow B). Likewise, oxidation from the folded geometry of the d^1 configuration

(62) A reviewer commented on the 5 kcal mol^{-1} difference in the barrier energies of the Mo and V d^1 configurations at 25°. Our calculated fragment wavefunction analysis suggests that this difference cannot be specifically ascribed to fragment energy matching and/or overlap effects of the fragment orbitals and that this energy difference is due to subtle differences between the Mo and V cases. In the d^0 electron configurations a larger barrier energy for V is also observed.

(63) Domercq, B.; Coulon, C.; Fourmigué, M. *Inorg. Chem.* **2001**, *40*, 371−378.

allows a low energy investment to the folded structure of the d^0 electronic configuration (arrow C). The coupling of paths B and C (green arrows and line) through the d^1 electron configuration results in a two-step two-electron oxidation of the d^2 to d^0 electron configuration with smaller barrier and reorganization energies. The shallow potential surface calculated for the d^1 electron configuration and the low frequency of the dithiolate folding motion provide an intermediate that can effectively link the d^2 and d^0 electron configurations and geometries. Thus, the potential curves of Figure 7 show how sequential one-electron transfers coupled to fold angle variation offer a reaction pathway for reoxidation of molybdenum enzymes with a lower overall energy barrier than two-electron oxidation without the d^1 configuration or the dithiolate-folding effect. These smaller energy barriers allow the reoxidation of the metal center to occur with concomitant electron transfer and change in the fold angle.

Conclusions

The vanadocene dithiolate systems compare well with previous studies of the titanocene and molybdocene dithiolate electronic structures,[22,47] thus completing the d^0, d^1, and d^2 configurations found in mononuclear molybdenum protein active sites. The crystallographic and computational data also support the change in fold angle upon filling the metal in-plane orbital.

Comparison of the PES of vanadocene systems with their respective titanocene analogues shows that their electronic structures are similar, with the exception of the extra electron in the vanadium complexes. For $Cp_2V(S_2C_2H_2)$ and Cp_2V(bdt), both the SOMO and the next lowest energy orbital show considerable vanadium and sulfur character, forming a bonding and antibonding pair. The SOMO is only half-filled, so the resulting contribution to the bond order from this interaction is one-half. The ΔSCF calculations compare well with the PES spectra of $Cp_2V(S_2C_2H_2)$ and Cp_2V(bdt) and place the SOMO as the lowest energy orbital.

The use of DFT calculations further supports the importance of the d^1 electronic configuration as a low-energy pathway for reoxidation of the metal center during catalysis. Two-electron oxidation of the d^2 electronic configuration to the d^0 configuration requires a larger relative energy investment for the removal of both electrons and geometric reorganization of the fold angle. The intermediate d^1 electronic configuration offers a low-energy pathway where a minimal amount of energy is required for reoxidation and geometric reorganization of the fold angle bridging the d^2 and d^0 electronic configurations.

The variation in dithiolate fold angle with formal d electron count observed for Cp_2M(dithiolates) supports the hypothesis that the change in the dithiolate fold angle effectively stabilizes d^0 and d^1 metal centers via π-donation from S_{π}^{+} to the M_{ip} orbital. This "dithiolate-folding effect" has implications for Mo/W enzymes since folding of the pyranopterin-dithiolate cofactor poises the metal center for reoxidation and geometric reorganization, modulating the reactivity of the enzyme active site as the metal center passes through the M(IV), M(V), and M(VI) formal oxidation states during electron and oxygen atom transfer.

Acknowledgment. We gratefully acknowledge support of this research by the National Institutes of Health (Grant GM-37773 to J.H.E.), a Galileo Circle Fellowship (M.A.C.), and the National Science Foundation (Grant CHE-0416004 to D.L.L. and Grant CHE-9601809 for the mass spectrometer). We thank Dr. A. Somogyi for mass spectrometry and Dr. Andrei Astashkin for the EPR spectra.

Supporting Information Available: Tables of optimized Cartesian coordinates, geometric structure parameters, and orbital composition for the complexes discussed, along with a potential energy curve, absorption spectrum, frozen solution EPR, and CIF file for $Cp_2V(S_2C_2H_2)$. This material is available free of charge via the Internet at http://pubs.acs.org.

IC701338S